Inorganic Chemistry

pubs.acs.org/IC
Article

Access of Adamantane-Type Organotin(IV) Heterochalcogenide Clusters

Jan Christmann, Niklas Rinn, Yannick J. Franzke,* and Stefanie Dehnen*

Cite This: https://doi.org/10.1021/acs.inorgchem.6c02451
Read Online

ABSTRACT: The access of metal chalcogenide clusters with tunable properties remains challenging. For a given geometric cluster structure, chemical and physical properties are defined by the exact composition. With a binary metal chalcogenide cluster core, one can reach a certain degree of tunability, but an even finer definition is possible by expanding the concept to ternary cluster composition. As a case example, we address adamantane-type organotin chalcogenide clusters of the general composition $[(RSn)_4E_6]$ (R = organic group, E = Se, Te) and herein report the targeted access of corresponding species exhibiting ternary clusters with two different types of chalcogen atoms involved, $[(RSn)_4E_{6-x}E'_x]$. We report three different methods for the synthetic access of E/E′ mixtures, including chalcogen exchange between preformed homochalcogenide clusters $[(RSn)_4E_6]$ and $[(RSn)_4E'_6]$ in solution. Extensive ^{119}Sn NMR studies on corresponding reaction mixtures with different ratios of the starting materials, in combination with sophisticated quantum chemical calculations of the chemical shifts, unambiguously confirm that all statistically possible clusters form in solution. Isolation of selected species in single-crystalline form also indicates the existence of ternary cluster cores with a narrow dispersion of species around the given E:E′ ratios. Our results represent an important step toward fine-tuning of metal chalcogenide cluster-based materials.

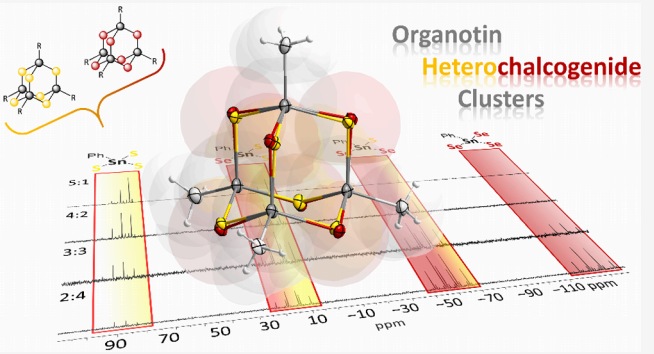

INTRODUCTION

Cluster compounds with an adamantane-type architecture are known for forming with nearly all elements of the periodic table. They feature photoluminescence,[1−4] electrochemical,[5] magnetic,[6,7] or catalytic[8,9] properties. Moreover, they have a high chemical stability due to their structure[10,11] and can be used as recyclable oxidation agents.[12]

Adamantane-type organo-group 14 chalcogenide clusters of the general formula $[(RTt)_4E_6]$ (R = organic group; Tt = Si, Ge, Sn; E = S, Se, Te) have attracted great attention owing to their ability to show extreme nonlinear optical properties in an amorphous state.[13−19] However, while these studies focused on the optical properties of the compounds, which indicated that the nature of R and E plays the most significant role, there has been a lack of structural information due to the inherent amorphous nature of most of these materials in most cases. Only recently, cocrystallization with C_{60} allowed for obtaining structural data from some of the intrinsically amorphous clusters.[20] A second aspect being barely addressed in these studies so far is the effect of mixed-chalcogenide compositions—with two different atom types of E being involved—on structural properties, in particular whether it might be possible to crystallize the compounds if the inorganic core gets more asymmetric (and thus, less isotropic) by introduction of different chalcogenide ligands.

We were therefore interested in exploring the possibility of introducing two types of chalcogenide atoms, namely, S, Se, or Te, into the adamantane-type core of corresponding organotin chalcogenide clusters. O atoms were not considered herein due to their tendency to form Sn/O ladder-type structures.[21,22]

The mixture of chalcogen ligands within cluster cores was previously reported for adamantane-type cadmium chalcogenolate species $[Cd_4(EPh)_{10}]^{2-}$ (E = S, Se); NMR-spectroscopic studies showed that a statistical mixture of clusters $[Cd_4(SR)_x(SeR)_{10-x}]$ was formed in solution by mixing the thiolate and selenolate precursors.[23] Similar observations were also reported for compounds based on orthostannates $[SnE_4]^{4-}$ or diorganotin chalcogenide oligomers $(R_2SnE)_3$, where an exchange of S with Se atoms afforded distinct NMR signals.[24,25] To the best of our knowledge, there are only two reports of adamantane-type organotin-based species exhibiting a mixed-chalcogenide situation. They bear either quaternary

Received: May 14, 2026
Revised: June 24, 2026
Accepted: June 30, 2026

cores of type $[(PhSn)_4(CH_2)_2E_4]$ (E = S, Se, Te) or ternary cores $[MeSi(PhSn)_3(CH_2)_3E_3]$ (E = S, Se).[26,27]

In organic chemistry, lighter congeners of chalcogen atoms have been replaced with heavier ones by using chalcogen substitution reagents, like Lawesson's or Woollins' reagent. These were applied to convert carbonyls to their respective thiocarbonyl or selones.[28,29] Similarly, the inorganic synthesis of monodisperse CdE (E = S, Se, Te) quantum dots made use of organophosphine chalcogenides as exchange reagents and cadmium carboxylates as metal sources.[30] The reactions thrive on the formation of the strong P−O bond, compared to the weaker P−E bonds.[31−33] This method can be used to transform Sn(II) and Pb(II) sulfides or selenides to their respective tellurides;[34] for group 10 selenide complexes, the chalcogenide exchange was accompanied by aggregations of metal ions and polytelluride formation.[35] Still, the use of substitution reagents could be a synthetic route to telluride-based clusters $[(RTt)_4Te_6]$,[36,37] which are difficult to access owing to their sensitivity toward light, moisture, and temperature and due to their low solubility.

Based on this knowledge, we aimed to find a straightforward approach for a general access toward heterochalcogenide clusters. Herein, we report the synthesis of organotin heterochalcogenide clusters $[(RSn)_4E_xE'_{x-6}]$ (R = Me, Ph; E/E′ = S/Se, Se/Te; x = 0−6), for which we explored three different methods (see Scheme 1). The first strategy revolves around reacting the respective homochalcogenide clusters with one another in solution. The second strategy is to exchange the chalcogen atoms of a given cluster with another congener using the respective organophosphine chalcogenide. The third strategy makes use of sodium chalcogenide of another congener for fragmenting a given cluster into the respective $Na_3[RSn(E/E')_3]$ salts and recombining it to a cluster molecule by addition of organotin trichloride.

Scheme 1. Schematic Overview of the Three Methods to Obtain Adamantane-Type Heterochalcogenide Clusters Reported Herein[a]

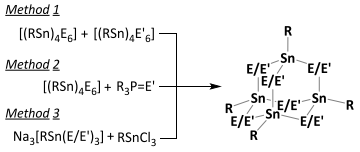

[a]Details on the stoichiometry of the reaction mixtures and on by-products are provided in the Experimental Section and in the main text.

EXPERIMENTAL SECTION

General

All synthetic steps were carried out under the exclusion of oxygen and moisture by use of standard Schlenk procedures using argon as an inert gas. $[(PhSn)_4E_6]$ (E = S, Se)[14] and nBu$_3$PTe[38] were prepared according to literature procedures. $[(MeSn)_4S_6]$ and $[(MeSn)_4Se_6]$ were prepared analogous to $[(PhSn)_4E_6]$. $(Me_3Si)_2E$ (E = S, Se, Te) were prepared with a modified literature synthesis[39,40] using Na_2E, prepared in liquid ammonia, as the starting material.

Synthesis of $[(MeSn)_4S_6]$ (C)

$MeSnCl_3$ (2.00 g, 8.18 mmol) was dissolved in 4 mL of toluene. TMS_2S (2.6 mL, 12.3 mmol) was slowly added, and the reaction was stirred overnight. The white solid was filtered and washed with 4 mL of n-hexane. The solid was further dried in vacuo, yielding 1.29 g (85.2% with respect to $MeSnCl_3$) of **C** as a colorless solid. ^{1}H NMR (THF-d_8, 500 MHz) δ = 1.11 (s, 3 H, ^2J (^{1}H−$^{117/119}$Sn) = 39.2 Hz) ppm. ^{119}Sn{^{1}H} (THF-d_8, 186.5 MHz): δ = 144.2 ($^2J_{Sn-C}$ = 128.7 Hz) ppm.

Synthesis of Heterochalcogenide Clusters $[(PhSn)_4S_xSe_{6-x}]$ (R = Me, Ph) via Method 1

$[(RSn)_4S_6]$ with R = Ph (**A**) or Me (**C**) (100 mg, 0.14 mmol/0.10 mmol) and different amounts (details of the exact molar ratios used are given in the main text) of $[(RSn)_4Se_6]$ with R = Ph (**B**) or Me (**D**) were stirred in the respective solvent (R = Ph:DCM, R = Me:DMF; 9 mL). The suspension was stirred for 16 h at room temperature. A clear solution of pale to bright yellow color formed during the reaction. The solution was used either directly for crystallization, or the solvent was removed under reduced pressure, and DCM-d_2 was added for NMR investigations. Single crystals of $[(MeSn)_4S_{3.30}Se_{2.74}]$ (**1**), $[(MeSn)_4S_{2.87}Se_{3.13}]$ (**2**), $[(MeSn)_4S_{1.28}Se_{4.72}]$ (**3**), and $[(MeSn)_4S_{0.84}Se_{5.16}]$ (**4**) were obtained by layering with 10 mL of Et_2O. With increased Se content, the color of the crystals deepened slightly, from pale yellow (**1**) to yellow (**4**).

Synthesis of Heterochalcogenide Clusters $[(PhSn)_4S_xSe_{6-x}]$ via Method 2

$[(PhSn)_4S_6]$ (**A**) (100 mg, 0.10 mmol) and different amounts of triphenylphosphine selenide were stirred in 20 mL of toluene (details of the exact molar ratios used are given in the Results and Discussion section). The suspension was heated to reflux conditions and stirred for 20 h. A yellow solid was formed during the reaction. From the cooled reaction solution, the solvent was removed under reduced pressure. The residue was dissolved in DCM-d_2 for further investigation.

Synthesis of Heterochalcogenide Clusters $[(PhSn)_4S_xTe_{6-x}]$ and $[(PhSn)_4Se_xTe_{6-x}]$ via Method 2

$[(PhSn)_4E_6]$ with E = S (**A**) or Se (**B**) (100−200 mg) and different amounts of tri-n-butylphosphine telluride were stirred in 20 mL of DCM or toluene at room temperature (details of the exact molar ratios used are given in the Results and Discussion section).

Synthesis of Heterochalcogenide Clusters $[(MeSn)_4Se_xTe_{6-x}]$ via Method 2

$[(MeSn)_4Se_{4.20}Te_{1.80}]$ (**5**) was synthesized by layering a solution of $[(MeSn)_4Se_6]$ (30 mg, 29.7 μmol) in 40 mL of THF with 8 mL of a solution of tri-n-butylphosphine telluride (17.1 mg, 52.3 μmol) in DCM at room temperature. The red single crystals of $[(MeSn)_4Se_{4.20}Te_{1.80}]$ (**5**) formed on the walls of the tube after 3 days. $[(MeSn)_4Se_{0.17}Te_{5.83}]$ (**6**) was synthesized by layering 7 mL of a saturated solution of $[(MeSn)_4Se_6]$ in THF with 7 mL of a solution of tri-n-butylphosphine telluride (15.1 mg, 45.6 μmol) in DCM. From the reaction solution, reddish brown single crystals of $[(MeSn)_4Se_{0.17}Te_{5.83}]$ (**5**) were obtained after 9 days.

Synthesis of Heterochalcogenide Clusters via Method 3

$[(MeSn)_4S_6]$ (**C**) (140 mg; 0.19 mmol) and Na_2Se (144 mg, 1.15 mmol) were stirred in 20 mL of acetonitrile for 16 h. The solid was filtered off the solution, washed with acetonitrile, and dried under vacuum. The white solid was used as is. 100 mg of $Na_3[MeSn(S/Se)_3]$ solid was suspended in 10 mL of THF and cooled to −78 °C. To the suspension, a cooled solution of 0.98 mg (0.40 mmol) of $MeSnCl_3$ in 10 mL of THF was added and stirred overnight. The suspension was filtered via a syringe filter. 5 mL of the solution was layered by 10 mL of n-hexane to obtain crystals of $[(MeSn)_4S_{2.74}Se_{3.26}]$ (**2'**).

https://doi.org/10.1021/acs.inorgchem.6c02451
Inorg. Chem. XXXX, XXX, XXX−XXX

Synthesis of $Na_3[MeSnS_3]\cdot 6H_2O$ ($7\cdot 6H_2O$)

A Schlenk flask was charged with **A** (100 mg, 0.137 mmol) and $Na_2S\cdot 9H_2O$ (212 mg, 0.883 mmol). 4 mL of degassed acetone and 1 mL of degassed water were added. The reaction was stirred for 16 h. The volatiles were removed by reduced pressure, leaving a colorless solid. This solid is likely to contain (a) the raw product and (b) residual starting materials, $[(MeSn)_4S_6]$ and Na_2S. Assuming that the reaction was quantitative and accounting for the excess of Na_2S used (4.8 mg), the reaction should have yielded (164.4 + 4.8) mg = 169.2 mg of **7**. We obtained 173.3 mg though, which is why we suggest that also the raw product contains some water. The susceptibility of **7** for water inclusion was confirmed by the crystal structure of $7\cdot 6H_2O$. Crystals of $7\cdot 6H_2O$ were obtained by layering a solution of the remainder in ethanol with hexane (1:1 v/v). ^{1}H NMR (D_2O, 500 MHz) δ = 0.54 (s, 3 H, ^2J (^{1}H−$^{117/119}$Sn) = 61.7 Hz) ppm. ^{119}Sn{^{1}H} (D_2O, 186.5 MHz): δ = 110.5 ppm.

Nuclear Magnetic Resonance (NMR) Spectroscopy

^{1}H, ^{13}C, ^{77}Se, and ^{119}Sn spectroscopy was carried out using a Bruker Avance III HD 250 MHz, Bruker Avance II 300 MHz, Bruker Avance Neo300NB, or Bruker Avance III HD 500 MHz spectrometer. The chemical shifts are given in ppm relative to the residual protons of deuterated solvents for ^{1}H spectra and relative to the solvent signal for the ^{13}C spectra. The chemical shift is given to tetramethylsilane (^{1}H, ^{13}C, and ^{29}Si), 85% phosphoric acid in H_2O (^{31}P), dimethylselenide (^{77}Se), and tetramethylstannane (^{119}Sn), 90% in $CDCl_3$. Heteronuclear NMR experiments were done with ^{1}H broadband decoupling, if not stated otherwise.

High-Resolution Electrospray Ionization (ESI) Mass Spectrometry

ESI mass spectra were acquired with an LTQ-FT Ultra mass spectrometer (Thermo Fisher Scientific). The resolution was set to 100000.

Elemental Analysis

Samples for CHN(S) analysis were prepared in tin crucibles under an argon atmosphere and measured with a vario MICRO CUBE (Elementar).

Micro-X-ray Fluorescence Spectroscopy (μXFS)

Samples were prepared under a thin layer of oil and transferred into a glovebox. Measurements of elements with atomic numbers >11 were performed on a M4 Tornado (Bruker) with a rhodium target X-ray tube and a silicon-drift detector. The evaluation of the data was done with the program Esprit. Upon deconvolution of the spectra, quantification of the elements was achieved based on Se K, Te L, and Sn L radiation.

Hirshfeld Analyses

Hirschfeld surface analyses were conducted with the Crystal Explorer software suite (ver. 17.5).[41,42]

Single-Crystal X-ray Diffraction (SC-XRD)

SC-XRD measurements were done on IPDS-2 and IPDS-2T area detector systems and a StadiVari diffractometer of STOE & Cie GmbH at 100 K. In the case of IPDS-2 and IPDS-2T, monochromatic Mo−K_α radiation (λ = 0.71073 Å) was used, and diffractometers were equipped with an Oxford Cryosystems module. For measurements with StadiVari, Cu−K_α radiation from a Xenocs Microfocus Source (λ = 0.15406 Å) and a Dectris Pilatus 300 K Si hybrid pixel array detector were used. The raw data was processed with the program X-Area from STOE & Cie GmbH. For scaling with absorption correction, the program STOE X-Area Lana was used. Structure solutions by dual space methods and full-matrix least-squares refinement against F2 were carried out using SHELXT15, SHELXL15, and OLEX2 software.[43−45]

Powder X-ray Diffraction (P-XRD)

P-XRD was measured on a STOE StadiMP diffractometer (STOE & Cie GmbH), which was equipped with a Cu−Kα (λ = 0.15406 Å) Xenocs Microfocus source, a curved focusing monochromator, and a Mythen-1k detector. The samples were measured in transmission mode and prepared on a 3M tape strip (Scotch tape). Data processing and generation of the simulated powder diffraction pattern from single crystal diffraction data were done with the software WinXPOW version 3.5.0.2 (STOE & Cie GmbH).

Quantum Chemical Analysis of Reaction Mixtures of A and B, $[(PhSn)_4S_xSe_{6-x}]$

All-electron relativistic density functional theory (DFT) calculations[46−49] were carried out with the (one-electron) exact two-component (X2C) Hamiltonian in the diagonal local approximation to the unitary decoupling transformation (DLU) and the NMR-tailored x2c-TZVPall-s basis set.[50] A finite nucleus model based on a Gaussian charge distribution[51] was applied for both the scalar potential and the vector potential. For spin−orbit calculations, the modified screened nuclear spin−orbit (mSNSO) approximation[52] was considered for the spin-dependent integrals and integral derivatives of the relativistically modified potential to account for the two-electron picture-change error. The PBE,[53] PBE0,[54] BH&HLYP,[55] and ωB97X-D[56] density functional approximations were chosen together with a medium-sized integration grid (grid size 3a).[50] For the hybrid functionals, a seminumerical exchange approximation was applied for the left-hand side of the response equations only.[57,58] The resolution of the identity approximation for the Coulomb integrals[59,60] (RI-J) was always used with tailored auxiliary basis sets.[50,61] Solvent effects were included with the conductor-like screening model (COSMO) for DCM (ε_r = 8.93) and a Gaussian charge model.[60,62] Self-consistent field (SCF) energies were converged up to 10^{-8} E_h, and response equations were solved with a criterion of 10^{-7} a.u. for the norm of the residuum.[63] Structures were optimized in four steps with the scalar-relativistic Hamiltonian, as the impact of spin−orbit coupling on the structure is minuscule. First, the structure was optimized at the semilocal PBE level. Second, the dispersion correction D4[64] was included. Third, COSMO was applied to account for the environment effects in solution. For the hybrid functionals, the structure was further refined at the PBE0 level with D4 and COSMO. No symmetry constraints were applied, and the initial structures were taken from the crystallographic determination. All calculations herein were carried out with TURBOMOLE.[65,66]

Quantum Chemical Analysis of Reaction Mixtures of A or B and nBu$_3$Pte, $[(PhSn)_4S_xTe_{6-x}]$, or $[(PhSn)_4Se_xTe_{6-x}]$

Computational studies of the NMR spectra were carried out using the same computational methods. Structures were obtained at the PBE-D4 and PBE0-D4 levels with COSMO (DCM).

Quantum Chemical Analysis of the Anion in $Na_3[MeSnS_3]$

Structures were optimized with COSMO (ε_r = 80.10 for water) with PBE-D4 and PBE0-D4. NMR shifts were calculated accordingly.

RESULTS AND DISCUSSION

Results of Experiments According to Method 1: Reactions of Two Homochalcogenide Clusters

We started with the phenyl-substituted clusters $[(PhSn)_4E_6]$, E = S (**A**) and Se (**B**), as these species are reasonably soluble in dichloromethane (DCM), enabling us to obtain NMR spectra to track the reaction progress. Suspensions of both clusters with ratios of **A**:**B** = 5:1, 4:2, 3:3, and 2:4 in DCM were stirred at room temperature for 16 h. During the course of the reactions, the suspensions turned clear solutions (notably, suspensions of pure homochalcogenide clusters persist over time for the same concentrations applied here). After 16 h, the solvent was exchanged with DCM-d_2, and ^{119}Sn NMR spectra were recorded on these solutions (Figure 1).

Overall, 20 different signals are observed between 100 and −120 ppm, including those of the precursors **A** at 83.2 ppm and **B** at 97.8 ppm (cf. the reported values, 84.3 and −100.0 ppm, respectively).[14,67] The signals are grouped in four

https://doi.org/10.1021/acs.inorgchem.6c02451
Inorg. Chem. XXXX, XXX, XXX−XXX

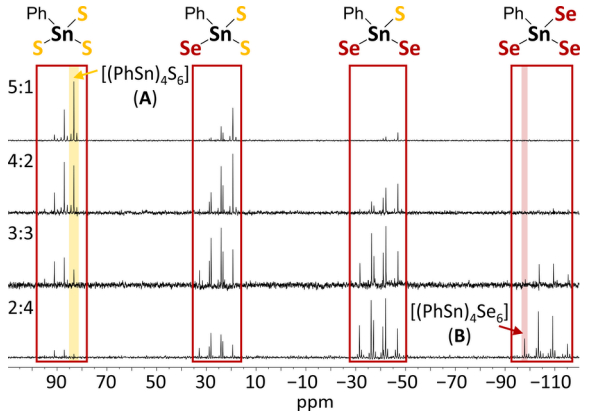

Figure 1. ^{119}Sn NMR spectra in DCM-d_2 of varied mixtures of clusters $[(PhSn)_4E_6]$, E = S (**A**), Se (**B**). The red boxes indicate signal groups that correspond to the illustrated nearest environments of the Sn atoms, $\{PhSnS_{3-x}Se_x\}$ (x = 0−3). The ^{119}Sn NMR signals of the $\{PhSnE_3\}$ unit for the homochalcogenide clusters **A** (E = S) and **B** (E = Se) are highlighted by yellow or red shaded areas. Corresponding signals for the heterochalcogenide clusters appear in the lower field (relative to **A**) or the higher field (relative to **B**).

regions, with a signal distribution of 4:6:6:4 in the 3:3 case, corresponding to a perfect statistical distribution. These regions cover 100 to 82 ppm, 35 to 10 ppm, −25 to −50 ppm, and −95 to −120 ppm (red boxes in Figure 1), and they are assigned to tin (hetero)chalcogenide units $\{RSnS_xSe_{3-x}\}$ with 3:0, 1:2, 2:1, and 3:0 ratios of S and Se.

From previous studies on heterochalcogenido metalate anions $[SnE_xE'_{4-x}]^{4-}$ (E = S, Se, Te; E′ = Se, Te), it is known that a higher content of heavier chalcogen congener causes the signals to appear at the higher field in the ^{119}Sn NMR spectrum, which also accords with the expectations in terms of the lower electronegativity of Se versus S.[25] Instead of four distinct signals for $\{PhSnS_3\}$, $\{PhSnS_2Se\}$, $\{PhSnSSe_2\}$, and $\{PhSnSe_3\}$, however, we observe the aforementioned groups of signals in four regions, indicating that secondary effects need to be taken into account. Within these groups, the additional presence of a heavier congener somewhere else in the cluster causes the signal to appear in the lower field, hence inverse to the effect caused by directly bonded Se versus S atoms. We were able to confirm this − initially unintuitive − trend with the help of quantum chemistry.

The secondary effects originate from the fact that the heterochalcogenide clusters $[(PhSn)_4S_xSe_{6-x}]$ are composed of a total of four $\{RSnS_xSe_{3-x}\}$ units. Hence, up to five species, **I**−**V**, with up to three constitutional isomers, **a**−**c**, can form theoretically, which add up to a total of nine different species. All of them are depicted in Scheme 2 and referred to as **I**, **IIa**+**b**, **IIIa**−**c**, **IVa**+**b**, and **V**. We would like to note that we cannot tell so far how the exchange of chalcogen atoms takes place mechanistically. Preliminary theoretical studies ruled out the most simple possibility of a spontaneous Sn−E[1] bond breaking occurring in a $[(RSn)_4S_6]$ cluster followed by nucleophilic attack of a tin atom of a neighboring $[(RSn)_4Se_6]$ cluster (or vice versa) and formation of an intermediate that temporarily comprises a {SnSSnSe} four-membered ring as a connecting unit. According to these studies, we need to assume that the process is much more complicated and likely to involve halide or Na^+ ions from the precursors and/or solvent molecules.

Scheme 2. All Possible Compositions and Constitutional Isomers of Heterochalcogenide Clusters $[(RSn)_4S_xSe_{6-x}]$

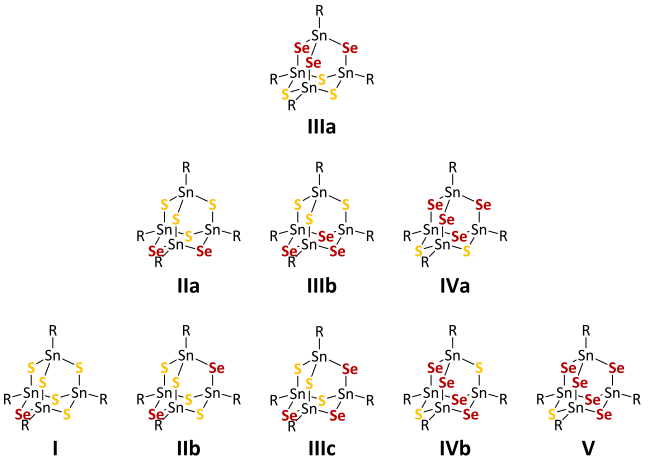

Assuming that each cluster gives an individual ^{119}Sn NMR signal for each of the chemically different $\{RSnS_xSe'_{6-x}\}$ units, 18 signals in total are expected. If those signals were to be grouped together in accordance with the S:Se ratio of atoms directly connected to the observed Sn nucleus, a signal pattern of 3:6:6:3 would be expected. Upon addition of the signals of the parent chalcogenide clusters, we obtain exactly the 4:6:6:4 pattern observed in the experimental spectrum of the equimolar solution (3:3) of **A** and **B**. So, we conclude that a statistical mixture of all possible species is actually formed in solution under exchange of the chalcogenide bridges upon opening of Sn−S and Sn−Se bonds and formation of new contacts. We note that the mechanism for this exchange has not yet been elucidated, but preliminary studies indicate a very complicated process involving multiple molecules, which will be investigated in detail in future work.

As an example, for the assignment of the individual signals in Figure 1 based on the species shown in Scheme 2, we take a closer look at the signals associated with the $\{RSnS_3\}$ units between 100 and 82 ppm (the leftmost red box in Figure 1). The corresponding signal found for the homosulfide cluster **A** at 83.2 ppm is located the farthest in the high field. This contrasts with what would be expected based on electronegativity alone, since by stronger deshielding of the Sn atom, the ^{119}Sn NMR signal of **A** should be the farthest in the low field. The influence of the neighboring Sn atoms, therefore, needs to be taken into account.

In a previous study on $[SnE_xE'_{4-x}]^{4-}$ anions (E = S, Se, Te; E′ = Se, Te), the ^{125}Te NMR and the ^{77}Se NMR spectra indicated a continuous shift toward the lower field for any substitution of Se by Te.[25] Based on the results from density functional theory calculations, it was concluded that this is due to different back bonding tendencies of the chalcogen atoms toward the tin neighbor. The lighter congener will mainly contribute to the back-donation with its widely nonbonding 3p (S) or 4p (Se) orbital. Thus, more electron density remains on the heavier congener, resulting in lower overall electron density on the Sn atom. Therefore, the ^{119}Sn NMR signals of $\{RSnS_3\}$ from clusters with a higher content of heavier congener are observed at chemical shifts in the relatively high field.

Due to the limited solubility of $[(PhSn)_4S_xSe_{6-x}]$ heterochalcogenide clusters, two-dimensional ^{119}Sn NMR experiments were not successful. Hence, in order to unambiguously

https://doi.org/10.1021/acs.inorgchem.6c02451
Inorg. Chem. XXXX, XXX, XXX−XXX

assign the signals shown in Figure 1 to the different species illustrated in Scheme 2, all-electron relativistic DFT calculations were carried out. Here, spin−orbit coupling is crucial for accurate results. In Figure 2, we outline the assignment of the three groups of signals to the species observed upon a 5:1 mixture of **A** and **B** as an example. Results for all species are summarized in Table S7.

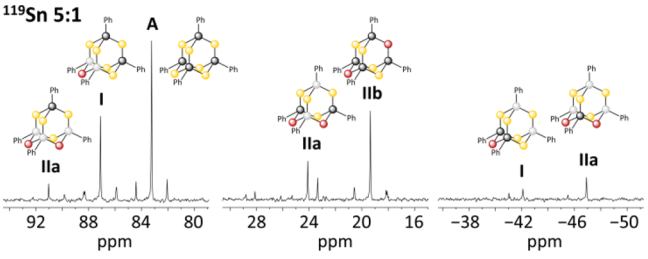

Figure 2. ^{119}Sn NMR spectrum of the 5:1 mixture of **A** and **B** in DCM-d_2. The assignment of the shown clusters to the respective signal is based on their distribution and intensity according to statistical abundance. The tin atoms that correspond to the indicated peaks are drawn in black (other ones in gray).

The range-separated hybrid functional ωB97X-D reproduced the experimental spectra in excellent agreement: all experimental signals were systematically underestimated by about 20 ppm, but a linear regression of the experimental shifts versus the calculated ones leads to a coefficient of determination of R^2 = 0.994 as shown in Figure 3.

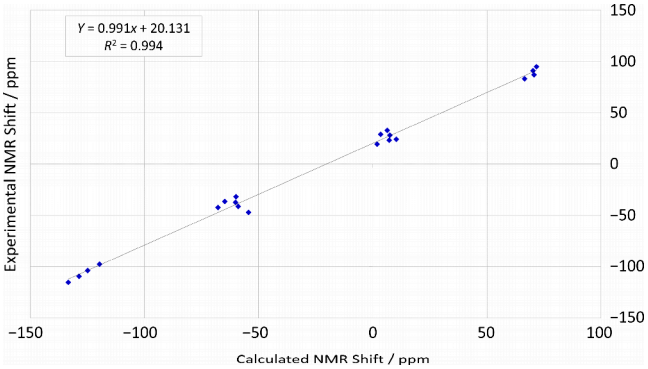

Figure 3. Plot of the calculated NMR shifts with relativistic all-electron DFT methods in ppm (x axis) versus the experimentally measured ones (y axis). The trend line is given along with the result of the linear fit.

As neither the parent compounds $[(PhSn)_4S_6]$ (**A**) and $[(PhSn)_4Se_6]$ (**B**) can be crystallized as pure compounds, nor has any other member of the series $[(PhSn)_4S_xS_{6-x}]$ showed any tendency to crystallize, we chose to run a second series of heterochalcogenide clusters for structural investigations. Based on the fact that $[(MeSn)_4E_6]$ with E = S (**C**) or Se (**D**) are known to form single crystals,[68,69] we used the methyl-decorated derivatives for this study. *N*,*N*-Dimethylformamide (DMF) was found to be a fairly suitable solvent. While it does not dissolve the parent compounds **C** and **D** individually, mixtures of both form clear solutions upon stirring overnight, similar to the observations made for mixtures of **A** and **B**. While the solubility and corresponding concentrations were still not sufficiently high to obtain ^{119}Sn NMR signals, crystallization experiments were successful. Upon layering the solution in DMF for the **C**:**D** ratios of 4:2, 3:2, 2:4, and 1:5 with Et_2O, pale yellow crystals suitable for SC-XRD were obtained; only for a **C**:**D** ratio of 5:1 that layering afforded amorphous powders.

All crystals were found to crystallize in the space group type $P\bar{1}$, like the selenide cluster **D**. As the crystal data of **C** and **D** were reported for room-temperature measurements,[68,47] we newly crystallized **C** and **D** and recorded SC-XRD data at 100 K for consistency with our experiments (see Table S2). The crystal structure refinement clearly revealed the presence of two types of chalcogenide bridges in the cluster molecules. Each chalcogen atom position can be refined as consisting of both S and Se atoms; atomic coordinates were refined individually (with anisotropic displacement parameters assumed to be equal for each S/Se pair sharing one position). Of course, X-ray diffraction experiments do not allow distinguishing between a coexistence of S and Se atoms within the same molecular unit on the one hand and a corresponding mixture of two clusters with only S or Se bridges on the other hand. However, as the NMR data that we obtained from the mixtures of **A** and **B** unambiguously proved the former to be the case upon exchange of chalcogenide bridges, we assume the same to be the case for the methyl-decorated species that we crystallized.

The elemental compositions of the single-crystalline products obtained from reaction mixtures of **C** and **D** with ratios of 4:2, 3:3, 2:4, and 1:5 are $[(MeSn)_4S_{3.25}Se_{2.75}]$ (**1**), $[(MeSn)_4S_{2.87}Se_{3.13}]$ (**2**), $[(MeSn)_4S_{1.28}Se_{4.72}]$ (**3**), and $[(MeSn)_4S_{0.85}Se_{5.15}]$ (**4**) (see Table S3) according to the crystal structure refinement. According to free refinement of the S:Se ratio, the content of S atoms is always somewhat lower than suggested from the composition of the reaction mixture. We therefore assume that the crystals contain a mixture of heterochalcogenide species, with a higher tendency for more Se-rich species to crystallize. The discrepancy of S content in the crystal and the corresponding reaction mixture is most pronounced in the case of the ratio 2:4 mixture, yielding crystals of compound **3** with a 1.28:4.72 ratio. Figure 4 illustrates the molecular structure of the cluster isolated from the 4:2 mixture of **C** and **D**, which was refined to the composition $[(MeSn)_4S_{3.25}Se_{2.75}]$ (**1**).

The preference of forming crystals with higher Se content is apparently connected to the difference in solubility of the homochalcogenide clusters, where a difference was observed between **C** and **D**. While traces of **C** can be observed by ^{1}H NMR spectrometry in deuterated THF at 1.11 ppm, no signal was observed for **D** in the same solvent, indicating its much poorer solubility. A higher sulfur content in the heterochalcogenide cluster is therefore assumed to increase the solubility and, in turn, suggests that more Se-rich clusters are more likely to precipitate (be it crystalline or noncrystalline). In addition, a higher crystallization tendency of **D** as compared to **C** was also confirmed by recrystallizing **C** and **D** from DMF by layering with Et_2O. Only **D** was obtained as visible crystals, while compound **C** formed an amorphous powdery solid instead. Another aspect worth mentioning is the mismatch in space group types between the **C** and **D**: all heterochalcogenide clusters $[(MeSn)_4S_xSe_{6-x}]$ crystallize in a structure that is isomorphic to that of the selenide cluster **D**, while the crystal structure type of **C** has not been observed for any of them. We suspect that for cluster mixtures, the packing pattern of the sulfide cluster is not favorable, which can be taken as another indication of the fact that more Se-rich clusters seem to be

https://doi.org/10.1021/acs.inorgchem.6c02451
Inorg. Chem. XXXX, XXX, XXX−XXX

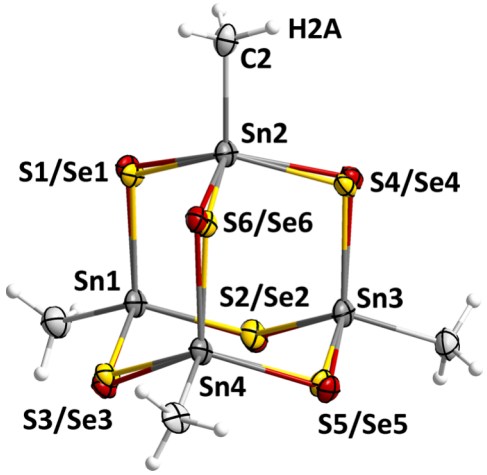

Figure 4. Molecular structure of the heterochalcogenide cluster $[(MeSn)_4S_{3.30}Se_{2.70}]$ (**1**). S and Se atoms were refined freely regarding the atom coordinates, as indicated by longer Sn−Se distances and shorter Sn−S distances. Thermal ellipsoids are shown at 50% probability.

favored in the mixtures. We note that none of the crystalline compounds **1**−**4** showed a solubility sufficient to record ^{119}Sn NMR spectra.

The Sn−E distances in **1**−**4** (E = S: 2.394(12)−2.444(19) Å; E = Se: 2.477(7)−2.5353(12) Å) are very similar to the ones reported for the homochalcogenide clusters **C** (Sn−S: 2.3943(6)−2.4044(7) Å) and **D** (Sn−Se: 2.518(2)−2.538(2) Å) (see Table S3). A very slight increase (on average) of the Sn−S distances when going from **1** to **4**, hence increasing the Se content, and a very slight decrease (on average) of the Sn−Se distance when going from **4** to **1**, hence increasing the S content, indicate that some of the disorder of S and Se atoms could not be resolved in the refinement, but the discrimination of the largest part of it is still clear.

Results of Experiments According to Method 2: Reactions of Homochalcogenide Clusters with Organophosphine Chalcogenides

As illustrated in Figure 5 (left), the treatment of **A** with triphenylphosphine selenide in a 1:6 ratio in toluene at reflux

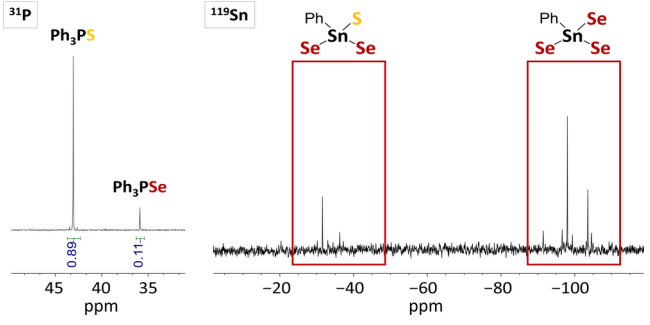

Figure 5. ^{31}P NMR spectrum of a mixture of **A** and Ph_3PSe in a 1:6 ratio in toluene and corresponding ^{119}Sn NMR spectrum in DCM-d_2.

conditions led to an 89% conversion of Ph_3P=Se to Ph_3P=S according to ^{31}P NMR spectroscopy (in contrast to reactions in DCM, which did not yield any conversion). In order to explore which species have formed this way, we recorded ^{119}Sn NMR spectra from the resulting reaction solution. The rather intense signals are observed in the regions that can be assigned to the $\{PhSnSSe_2\}$ and $\{PhSnSe_3\}$ groups (cf. Figure 1). The leftmost signal in the high-field region (−97.8 ppm; along with its Sn−Se satellites at −91.3 ppm and −104.3 ppm) stems from **B**. The two other signals (−103.4 and −31.4 ppm) can be assigned to species **V**.

When investigating reaction mixtures of **A** with 2, 3, or 4 equiv of Ph_3P=Se by ^{119}Sn NMR spectroscopy, the spectra show multiple signals in accordance with the observations made with Method 1 (Figure 1). An excess of a total of 10 equiv of Ph_3P=Se yields conversion to **B** and minor decomposition. The complete collection of NMR data from the reactions with Ph_3P=Se can be found in the Supporting Information (Figure S6).

In the next step, we wanted to test whether this method can also be utilized to introduce tellurium into **A**, **B**, **C**, or **D**. The respective homotelluride clusters $[(RSn)_4Te_6]$ (R = Me, Ph) have not yet been reported in the literature. The conventional synthesis route for $[(RSn)_4E_6]$ (R = Me, Ph), starting from organotin trichloride and bis(trimethylsilyl) chalcogenide, did yield in fast precipitation of a red amorphous solid that was insoluble in our solvents or showed signs of decomposition. Therefore, we decided to take a different approach and use organophosphine telluride.

We therefore reacted **A** with nBu$_3$P=Te at room temperature and monitored the conversion of nBu$_3$P=Te to nBu$_3$P=S by ^{31}P NMR spectroscopy again (Figure 6, left). As for the exchange

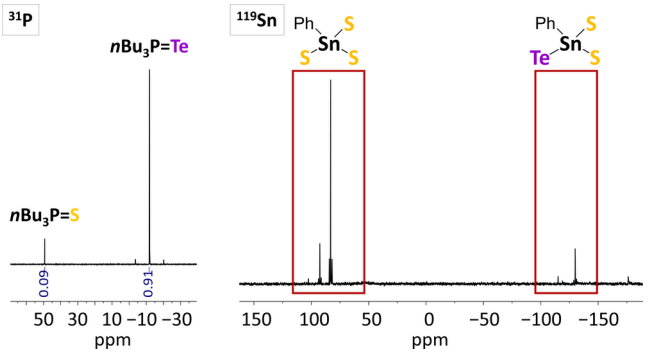

Figure 6. ^{31}P NMR spectrum of a mixture of **A** and nBu$_3$P=Te in a 1:6 ratio in DCM-d_2 and corresponding ^{119}Sn NMR spectrum.

with Se, we found the conversion to be solvent-dependent. In DCM, the reaction with 6 equiv of nBu$_3$P=Te did not exceed 8.6% conversion, although no precipitation was taking place, which would indicate kinetic hindrance. The respective ^{119}Sn NMR spectrum (Figure 6, right) shows five signals, which we assign to clusters $[(PhSn)_4S_xTe_{6-x}]$ in analogy to the $[(PhSn)_4S_xSe_{6-x}]$ system. The S/Te analogue of **I**, $[(PhSn)_4S_5Te]$, is expected to cause two signals, which are found at +92.6 and −129.9 ppm. Here, our relativistic DFT calculations yield +94.2 and −129.7 ppm, clearly supporting the assignment (see Table S8). The remaining signals do not fit the Te-analogues of **IIa** $[(PhSn)_4S_4Te_2]$ as the signal of the $\{PhSnSTe_2\}$ unit is expected to be shifted further to the high field. Based on the computational studies (Table S8), we would expect signals at 98.2, −104.6, and −335.1 ppm for the $\{PhSnS_3\}$, $\{PhSnS_2Te\}$, and $\{PhSnSTe_2\}$ units in **IIa**, respectively. Also, the isomer **IIb** should have a higher intensity compared to **IIa**. The formation of other heterochalcogenide cluster species in this system can be excluded as conversion from nBu$_3$P=Te to nBu$_3$P=S came to a hold and a

https://doi.org/10.1021/acs.inorgchem.6c02451
Inorg. Chem. XXXX, XXX, XXX−XXX

statistical formation of heterochalcogenide clusters is assumed. Hence, first, the formation of **IIa** and **IIb** had to be observed before Te-richer species are formed. As the additional signals do not fit with any other heterochalcogenide species, these signals might indicate the dissociation of the molecule in solution, which was also reported for $[Sn_4Te_{10}]^{4-}$.[70]

The same reaction conducted in toluene yielded an orange-yellow solution and some red solids after 21 h. After 72 h, we observed a conversion of about 63%. Increasing the reaction temperature to reflux yielded full conversion of nBu$_3$P=Te, but it also led to the formation of black SnTe, which was identified by powder X-ray diffraction (PXRD) (see Figure S9).

For the reaction of **B** with nBu$_3$P=Te, a similar behavior was found in toluene. However, in DCM, the reaction with 6 equiv of nBu$_3$P=Te leads to a conversion to nBu$_3$P=Se of up to approximately 55% alongside the formation of an insoluble amorphous red solid (see the PXRD results in Figure S10), which according to X-ray fluorescence spectroscopy (μ-XFS) showed the presence of Sn, Se, and Te in a ratio of 1:0.81:1.12 (see Figure S12). This deviates from the Sn:Se + Te ratio of 1:1.5 expected for adamantane-type compounds. A reason for the deviation could be the partial overlap of L-series of Sn and Te, which interferes in the quantification by deconvolution or by partial absorption of emission of tin by Te. An initial exchange between of Se atoms in **B** with Te atoms could have taken place, but the extent of the exchange and potential follow-up reactions (including decomposition) of the exchanged product remain unclear.

Decreasing the ratio of nBu$_3$P=Te to 1 equiv leads to full conversion to the respective selenide. Besides the signal of **B** at −97.8 ppm, the ^{119}Sn NMR spectrum in DCM-d_2 showed three additional signals (Figure 7). The signal at −88.6 ppm is

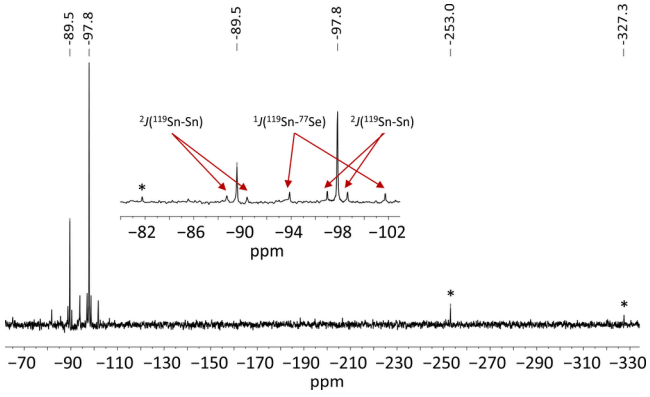

Figure 7. ^{119}Sn NMR spectrum of a mixture of **B** and nBu$_3$P=Te in a 1:1 ratio in DCM-d_2. The two asterisks indicate signals that would fit the predicted chemical shifts (DFT) for the Se/Te analogue of **1** rather well but do not show the expected intensities.

shifted to the low field as compared to that for **B** as expected for the {RSnSe$_3$} unit in the heterochalcogenide cluster [(PhSn)$_4$Se$_5$Te] (hence, the Se/Te analogue of **I**), but we were unable to detect its {RSnSe$_2$Te} counterpart, which should show a similar signal intensity. DFT calculations of [(PhSn)$_4$Se$_5$Te] predict chemical shifts of −94.1 and −245.2 ppm for the two units. Therefore, we also assume dissociation of the molecule into smaller units in solution, as pointed out before. μ-XFS analysis of the dried reaction residue showed a ratio of 1:1.24:0.22 (Sn/Se/Te) (see Figure S11).

As analysis in solution has proven to be difficult, we aimed to crystallize the Se/Te heterochalcogenide clusters by using [(MeSn)$_4$Se$_6$] (**D**) as the starting material. Reacting a supernatant solution of **D** in THF with 2 equiv of nBu$_3$P=Te yielded a few dark red crystals after 3 days. From the crystal structure analysis, an arrangement isostructural to **D** was obtained with a crystallographic composition of [(MeSn)$_4$Se$_{4.22}$Te$_{1.77}$] (**5**). Reacting a saturated solution of **D** with an excess of nBu$_3$P=Te yielded dark crystals with a crystallographic composition of [(MeSn)$_4$Se$_{0.17}$Te$_{5.83}$] (**6**). In both cases, tellurium was incorporated into the adamantane-type clusters. The Sn−Te distances in the clusters are in good agreement with those reported for [(R^{Mo}Sn)$_4$Te$_6$] (R^{Mo} = {Cp(CO)$_3$Mo})[37] (see Table S4). The composition of the crystals of **6** was confirmed by μ-XFS (see Figure S13), while crystals of **5** were too thin to be studied by this technique.

We conclude that method 2 did allow us to form heterochalcogenide clusters with S and Te or Se and Te bridges, up to high Te contents. A homotelluride species does not obviously form this way.

Method 3: Reconstruction of Clusters from a (Hetero)Chalcogenido Stannate and an Organotin Trichloride

Adamantane-type clusters can be fragmented by addition of sodium chalcogenide to their organotin chalcogenide salts, such as Na$_3$[PhSnE$_3$].[71,72] In a similar way, we synthesized the new salt Na$_3$[MeSnS$_3$]·6 H$_2$O (**7**·6H$_2$O) by reaction of [(MeSn)$_4$S$_6$] (**C**) with 6 equiv of Na$_2$S. It was characterized by ^{1}H and ^{119}Sn NMR spectroscopy in D$_2$O and obtained as single-crystals suitable for X-ray diffraction. **7**·6H$_2$O crystallizes in the orthorhombic crystal system, space group type *Pmma*, with 4 formula units in the unit cell. The molecular unit [MeSnS$_3$]$^{3-}$ possesses crystallographic C_s symmetry, and we refine two crystallographic inequivalent sodium atoms, Na1 and Na2. Na1 is coordinated in a (distorted) square-pyramidal manner (Na1···S$_3$O$_2$), and the coordination environment of Na2 represents a distorted octahedron (Na2···S$_2$O$_4$) through sulfur atoms from the [MeSnS$_3$]$^{3-}$ anion and water molecules (Figure 8).

To obtain a heterochalcogenide cluster from a corresponding heterochalcogenide anion [MeSn(S/Se)$_3$]$^{3-}$, compound **C** was stirred with 6 equiv of Na$_2$Se in acetonitrile for 16 h. The washed insoluble residue was used to react with 1 equiv of

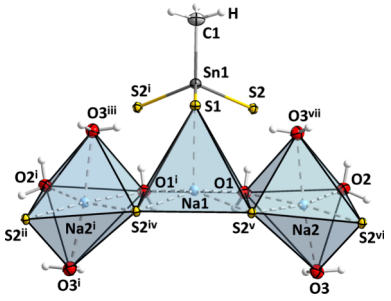

Figure 8. Cut-out of the crystal structure of Na$_3$[MeSnS$_3$]·6H$_2$O (**7**·6H$_2$O), illustrating the coordination polyhedra around the Na$^+$ ions and their further connection to other anions. Symmetry-equivalent atoms are generated according to the following operations: i = x, 1/2 − y, z; ii = 1/2 − x, −1/2 + y, 1/2 + z; iii = 1/2 − x, −1/2 + y, −1/2 + z; iv = −1/2 + x, 1/2 − y, 3/2 − z; v = −1/2 + x, y, 3/2 − z; vi = 1/2 − x, 1 − y, 1/2 + z; vii = 1/2 − x, 1 − y, −1/2 + z. Thermal ellipsoids are shown at 50% probability.

https://doi.org/10.1021/acs.inorgchem.6c02451
Inorg. Chem. XXXX, XXX, XXX−XXX

$MeSnCl_3$ in THF. Layering of the filtered reaction solution with *n*-hexane afforded single crystals. SC-XRD measurement revealed another heterochalcogenide cluster of similar composition as **1** but different cell parameters, $[(MeSn)_4S_{2.74}Se_{3.26}]$, which we refer to as compound **2′** (see Table S2). This proves that method 3 can also be used to form heterochalcogenide clusters. However, compared to method 1, it is far more time- and solvent-consuming and was therefore not pursued further.

SUMMARY AND CONCLUSIONS

This study focused on establishing synthetic routes toward adamantane-type organotin(IV) heterochalcogenide clusters $[(RSn)_4E_xE'_{6-x}]$ (R = Ph, Me; E/E′ = S/Se, S/Te, Se/Te) and on a detailed analysis of their compositions. This way, we hoped to get access to compounds with finely tunable compositions of their semiconductor-derived cluster cores.

Three methods have been tested and compared, and heterochalcogenide clusters combining S and Se atoms, $[(RSn)_4S_xSe_{6-x}]$, were successfully synthesized through all three methods, but the reaction of two homochalcogenide clusters $[(RSn)_4E_6]$ and $[(RSn)_4E'_6]$ (method 1) and the reaction of a homochalcogenide cluster based on chalcogen E with $Ph_3P{=}E'$ comprising the other type of chalcogen atom (method 2) turned out to be the practically preferred routes.

Method 1 delivered 9 cluster species in mixtures of perfectly statistical distributions, which were distinguishable by detailed ^{119}Sn NMR spectroscopy for R = Ph. Assignment of the signals was done based on the literature data for the parent systems $[(RSn)_4S_6]$ and $[(RSn)_4Se_6]$ in combination with highly sophisticated DFT calculations of the chemical shifts of all species. With R = Me, some of the species could be crystallized as heterochalcogenide cluster mixtures (**1**−**4**) − with a higher crystallization tendency of the more Se-rich species. Using $Ph_3P{=}E'$ according to method 2 allowed us to explore heterochalcogenide clusters involving Te atoms, $[(RSn)_4E_xTe_{6-x}]$ (E = S, Se). This enabled access to rather tellurium-rich clusters and also in crystalline form (**5** and **6**). The route might be promising as a generally applicable synthesis pathway for the yet sparsely investigated organotetrel telluride clusters $[(RTt)_4Te_6]$ (R = organic group; Tt = Si, Ge, Sn), but it is worth noting that generally, there seems to be an increased tendency for decomposition of the Te-based species.

Method 3 is a two-step approach starting with the fragmentation of the parent cluster $[(RSn)_4E_6]$ into an anionic fragment $[RSn(E/E')_3]^{3-}$ by treatment with Na_2E' followed by reaction of the latter with $RSnCl_3$. The methods turned out to deliver a heterochalcogenide cluster similar to **1**, but it is far less efficient regarding preparation times and the amount of solvent required.

All in all, this study proves that these clusters, which were heretofore considered to be rather inert, undergo rapid chalcogenide exchange with each other and other sources of chalcogenides in solution. Future work will be conducted to understand the mechanism of such exchange reactions that appear to be rather complicated on the basis of preliminary studies. In addition, future studies will be dedicated to the optical properties of the heterochalcogenide clusters, which are likely to represent a combination of the properties of the parent compounds, hence giving us a means of tailoring the absorption bands of the mixture.

ASSOCIATED CONTENT

Supporting Information

The Supporting Information is available free of charge on the ACS Publications Web site. The Supporting Information is available free of charge at https://pubs.acs.org/doi/10.1021/acs.inorgchem.6c02451.

All NMR spectra, synthetic methods and procedures, and main computational results (PDF)

Complete computational data (ZIP)

Accession Codes

Deposition Numbers 2553936−2553945 contain the supplementary crystallographic data for this paper. These data can be obtained free of charge via the joint Cambridge Crystallographic Data Centre (CCDC) and Fachinformationszentrum Karlsruhe Access Structures service.

AUTHOR INFORMATION

Corresponding Authors

Yannick J. Franzke − *Institute of Nanotechnology, Karlsruhe Institute of Technology (KIT), 76131 Karlsruhe, Germany; Otto Schott Institute of Materials Research, Friedrich Schiller University Jena, 07743 Jena, Germany;* orcid.org/0000-0002-8344-113X; Email: yannick.franzke@kit.edu

Stefanie Dehnen − *Institute of Nanotechnology, Karlsruhe Institute of Technology (KIT), 76131 Karlsruhe, Germany;* orcid.org/0000-0002-1325-9228; Email: stefanie.dehnen@kit.edu

Authors

Jan Christmann − *Institute of Nanotechnology, Karlsruhe Institute of Technology (KIT), 76131 Karlsruhe, Germany*

Niklas Rinn − *Institute of Nanotechnology, Karlsruhe Institute of Technology (KIT), 76131 Karlsruhe, Germany*

Complete contact information is available at: https://pubs.acs.org/10.1021/acs.inorgchem.6c02451

Notes

The authors declare no competing financial interest.

ACKNOWLEDGMENTS

The authors gratefully acknowledge financial support from the Deutsche Forschungsgemeinschaft (DFG, German Research Foundation) within the framework of the Research Unit "Amorphous Molecular Materials with Extreme Non-Linear Optical Properties" (FOR 2824, project number 398143140), project A1. This work was partly carried out with the support of the Karlsruhe Nano Micro Facility (KNMFi, www.knmf.kit.edu), an Open Access Research Infrastructure within the Karlsruhe High Technology Hub at the Karlsruhe Institute of Technology (KIT − The University in the Helmholtz Association, www.kit.edu). Y.J.F. gratefully acknowledges financial support via the Walter−Benjamin Programme funded by the Deutsche Forschungsgemeinschaft (DFG, German Research Foundation) — 518707327. We thank Dr. Frank Tambornino for help with the X-ray structure refinements.

REFERENCES

(1) Artem'ev, A. V.; Davydova, M. P.; Berezin, A. S.; Samsonenko, D. G.; Bagryanskaya, I. Y.; Brel, V. K.; Hei, X.; Brylev, K. A.; Artyushin, O. I.; Zelenkov, L. E.; Shishkin, I. I.; Li, J. New Approach

toward Dual-Emissive Organic−Inorganic Hybrids by Integrating Mn(II) and Cu(I) Emission Centers in Ionic Crystals. *ACS Appl. Mater. Interfaces* **2022**, *14* (27), 31000−31009.
(2) Chen, S.; Gao, J.; Chang, J.; Li, Y.; Huangfu, C.; Meng, H.; Wang, Y.; Xia, G.; Feng, L. Family of Highly Luminescent Pure Ionic Copper(I) Bromide Based Hybrid Materials. *ACS Appl. Mater. Interfaces* **2019**, *11* (19), 17513−17520.
(3) Jalilian, E.; Liao, R.-Z.; Himo, F.; Brismar, H.; Laurell, F.; Lidin, S. Luminescence Properties of the $Cu_4I_6^{2-}$ Cluster. *CrystEngComm* **2011**, *13* (14), 4729.
(4) Soloviev, V. N.; Eichhöfer, A.; Fenske, D.; Banin, U. Size-Dependent Optical Spectroscopy of a Homologous Series of CdSe Cluster Molecules. *J. Am. Chem. Soc.* **2001**, *123* (10), 2354−2364.
(5) Lin, J.; Dong, Y.; Zhang, Q.; Hu, D.; Li, N.; Wang, L.; Liu, Y.; Wu, T. Interrupted Chalcogenide-Based Zeolite-Analogue Semiconductor: Atomically Precise Doping for Tunable Electro-/Photoelectrochemical Properties. *Angew. Chem., Int. Ed.* **2015**, *54* (17), 5103−5107.
(6) Cook, A. W.; Bocarsly, J. D.; Lewis, R. A.; Touchton, A. J.; Morochnik, S.; Hayton, T. W. An Iron Ketimide Single-Molecule Magnet $[Fe_4(N{=}CPh_2)_6]$ with Suppressed through-Barrier Relaxation. *Chem. Sci.* **2020**, *11* (18), 4753−4757.
(7) Dubé, C. E.; Wright, D. W.; Pal, S.; Bonitatebus, P. J.; Armstrong, W. H. Tetranuclear Manganese-Oxo Aggregates Relevant to the Photosynthetic Water Oxidation Center. Crystal Structure, Spectroscopic Properties and Reactivity of Adamantane-Shaped $[Mn_4O_6(Bpea)_4]^{4+}$ and the Reduced Mixed-Valence Analog $[Mn_4O_6(Bpea)_4]^{3+}$. *J. Am. Chem. Soc.* **1998**, *120* (15), 3704−3716.
(8) Zhong, M.; Yang, Z.; Yi, Y.; Zhang, D.; Sun, K.; Roesky, H. W.; Yang, Y. Tin Sulfide and Selenide Clusters Soluble in Organic Solvents with the Core Structures of Sn_4S_6 and Sn_4Se_6. *Dalton Trans.* **2015**, *44* (46), 19800−19804.
(9) Sun, H.; Harms, K.; Sundermeyer, J. Aerobic Oxidation of 2,3,6-Trimethylphenol to Trimethyl-1,4-Benzoquinone with Copper(II) Chloride as Catalyst in Ionic Liquid and Structure of the Active Species. *J. Am. Chem. Soc.* **2004**, *126* (31), 9550−9551.
(10) Wieghardt, K.; Bossek, U.; Nuber, B.; Weiss, J.; Bonvoisin, J.; Corbella, M.; Vitols, S. E.; Girerd, J. J. Synthesis, Crystal Structures, Reactivity, and Magnetochemistry of a Series of Binuclear Complexes of Manganese(II), -(III), and -(IV) of Biological Relevance. The Crystal Structure of $[L'Mn^{IV}(\mu\text{-}O)_3Mn^{IV}L'](PF_6)\bullet 2H_2O$ Containing an Unprecedented Short Mn•••Mn Distance of 2.296 Å. *J. Am. Chem. Soc.* **1988**, *110* (22), 7398−7411.
(11) Homer, G. D.; Sommer, L. H. Reactivity Studies of Bridgehead Organosilicon Compounds with Nucleophilic Reagents. *J. Am. Chem. Soc.* **1973**, *95* (23), 7700−7707.
(12) Tohma, H.; Maruyama, A.; Maeda, A.; Maegawa, T.; Dohi, T.; Shiro, M.; Morita, T.; Kita, Y. Preparation and Reactivity of 1,3,5,7-Tetrakis[4-(Diacetoxyiodo)Phenyl]Adamantane, a Recyclable Hypervalent Iodine(III) Reagent. *Angew. Chem., Int. Ed.* **2004**, *43* (27), 3595−3598.
(13) Rosemann, N. W.; Eußner, J. P.; Beyer, A.; Koch, S. W.; Volz, K.; Dehnen, S.; Chatterjee, S. A Highly Efficient Directional Molecular White-Light Emitter Driven by a Continuous-Wave Laser Diode. *Science* **2016**, *352* (6291), 1301−1304.
(14) Dornsiepen, E.; Dobener, F.; Chatterjee, S.; Dehnen, S. Controlling the White-Light Generation of $[(RSn)_4E_6]$: Effects of Substituent and Chalcogenide Variation. *Angew. Chem., Int. Ed.* **2019**, *58* (47), 17041−17046.
(15) Rosemann, N. W.; Eußner, J. P.; Dornsiepen, E.; Chatterjee, S.; Dehnen, S. Organotetrel Chalcogenide Clusters: Between Strong Second-Harmonic and White-Light Continuum Generation. *J. Am. Chem. Soc.* **2016**, *138* (50), 16224−16227.
(16) Hanau, K.; Schwan, S.; Schäfer, M. R.; Müller, M. J.; Dues, C.; Rinn, N.; Sanna, S.; Chatterjee, S.; Mollenhauer, D.; Dehnen, S. Towards Understanding the Reactivity and Optical Properties of Organosilicon Sulfide Clusters. *Angew. Chem., Int. Ed.* **2021**, *60* (3), 1176−1186.
(17) Pilgrim, W.-C.; Stellhorn, J. R.; Klee, B. D.; Vasco, J. L.; Paulus, B.; Zeidler, A.; Hosokawa, S.; Hayakawa, S.; Dehnen, S. Structure Determination in a New Class of Amorphous Cluster Compounds with Extreme Nonlinear Optical Properties. *J. Phys. Soc. Jpn.* **2022**, *91* (9), No. 091004.
(18) Klee, B. D.; Paulus, B.; Link Vasco, J.; Hosokawa, S.; Stellhorn, J. R.; Hayakawa, S.; Dehnen, S.; Pilgrim, W.-C. Origin of Crystallization Suppression in a New Amorphous Molecular White-Light-Generating Material. *Scr. Mater.* **2022**, *219*, No. 114851.
(19) Rojas-León, I.; Christmann, J.; Schwan, S.; Ziese, F.; Sanna, S.; Mollenhauer, D.; Rosemann, N. W.; Dehnen, S. Cluster-Glass for Low-Cost White-Light Emission. *Adv. Mater.* **2022**, *34* (33), No. 2203351.
(20) Wang, Y.; Rinn, N.; Eberheim, K.; Ziese, F.; Christmann, J.; Jana, A.; Nier, S.; Rosemann, N. W.; Sanna, S.; Dehnen, S. The π-Trap Approach for Obtaining Crystal Structure Data of Inherently Amorphous Cluster Compounds. *Nat. Commun.* **2025**, *16* (1), 7903.
(21) Harrison, P. G.; Begley, M. J.; Molloy, K. C. The Mössbauer Recoil-Free Fraction and Structure. *J. Organomet. Chem.* **1980**, *186* (2), 213−236.
(22) Schiwy, W.; Krebs, B. $Sn_{10}O_4S^{8-}{}_{20}$: A New Type of Polyanion. *Angew. Chem., Int. Ed. Engl.* **1975**, *14* (6), 436−436.
(23) Dean, P. A. W.; Vittal, J. J. Cadmium-113 Nuclear Magnetic Resonance Spectroscopic Study of Mixed-Ligand Tetranuclear Clusters of the Type $[Cd_4(EPh)_x(E'R)_{10-x}]^{2-}$ and of the Mixed-Metal Clusters $[Cd_4Zn_{4-x}(SPh)_{10}]^{2-}$. *Inorg. Chem.* **1986**, *25* (4), 514−519.
(24) Blecher, A.; Mathiasch, B.; Mitchell, T. N. Fourier Transform Nmr Investigations of Organotin Compounds. *J. Organomet. Chem.* **1980**, *184* (2), 175−180.
(25) Ruzin, E.; Zent, E.; Matern, E.; Massa, W.; Dehnen, S. Syntheses, Structures, and Comprehensive NMR Spectroscopic Investigations of Hetero-Chalcogenidometallates: The Right Mix toward Multinary Complexes. *Chem.—Eur. J.* **2009**, *15* (21), 5230−5244.
(26) Dakternieks, D.; Jurkschat, K.; Wu, H.; Tiekink, E. R. T. Synthesis, Structure, and Exchange Reactions of New Stannaadamantanes Containing Chalcogenides. *Organometallics* **1993**, *12* (7), 2788−2793.
(27) Ayari, J.*Tripod-Shaped Organotin Compounds: Complexation Studies towards Lewis Bases and Chalcogenido Clusters of Unprecedented Nuclearity*. Disseration, Technische Universität Dortmund, Dortmund, 2020.
(28) Pedersen, B. S.; Scheibye, S.; Nilsson, N. H.; Lawesson, S.-O. Studies on Organophosphorus Compounds XX. Syntheses of Thioketones. *Bull. Soc. Chim. Belg.* **1978**, *87* (3), 223−228.
(29) Bhattacharyya, P.; Woollins, J. D. Selenocarbonyl Synthesis Using Woollins Reagent. *Tetrahedron Lett.* **2001**, *42* (34), 5949−5951.
(30) Murray, C. B.; Norris, D. J.; Bawendi, M. G. Synthesis and Characterization of Nearly Monodisperse CdE (E = Sulfur, Selenium, Tellurium) Semiconductor Nanocrystallites. *J. Am. Chem. Soc.* **1993**, *115* (19), 8706−8715.
(31) Capps, K. B.; Wixmerten, B.; Bauer, A.; Hoff, C. D. Thermochemistry of Sulfur Atom Transfer. Enthalpies of Reaction of Phosphines with Sulfur, Selenium, and Tellurium, and of Desulfurization of Triphenylarsenic Sulfide, Triphenylantimony Sulfide, and Benzyl Trisulfide. *Inorg. Chem.* **1998**, *37* (12), 2861−2864.
(32) Chernick, C. L.; Skinner, H. A.; Mortimer, C. T. Thermochemistry of Organophosphorus Compounds. Part I. Trimethyl and Triethyl Phosphites. *J. Chem. Soc.* **1955**, 3936.
(33) Liu, H.; Owen, J. S.; Alivisatos, A. P. Mechanistic Study of Precursor Evolution in Colloidal Group II−VI Semiconductor Nanocrystal Synthesis. *J. Am. Chem. Soc.* **2007**, *129* (2), 305−312.
(34) Sines, I. T.; Vaughn, D. D.; Biacchi, A. J.; Kingsley, C. E.; Popczun, E. J.; Schaak, R. E. Engineering Porosity into Single-Crystal Colloidal Nanosheets Using Epitaxial Nucleation and Chalcogenide

https://doi.org/10.1021/acs.inorgchem.6c02451
Inorg. Chem. XXXX, XXX, XXX−XXX

Anion Exchange Reactions: The Conversion of SnSe to SnTe. *Chem. Mater.* **2012**, *24* (15), 3088−3093.
(35) McConnachie, J. M.; Bollinger, J. C.; Ibers, J. A. Chalcogenide Substitution Reactions. *Inorg. Chem.* **1993**, *32* (18), 3923−3927.
(36) Schwedtmann, K.; Hepp, A.; Schwedtmann, K.; Weigand, J. J.; Lips, F. Amido Silicon Chalcogenide Compounds with Unprecedented Cluster Cores and Low Oxidation State Silicon Atoms. *Eur. J. Inorg. Chem.* **2019**, *2019* (44), 4719−4726.
(37) Merzweiler, K.; Kraus, H. Neue Metallorganisch Substituierte Zinn-Tellur-Verbindungen. Synthese Und Kristallstrukturen von $[\{Cp(CO)_2Fe\}_4Sn_2Te_2]$, $[\{Cp(CO)_3Mo\}_4Sn_2Te_2]$ Und $[\{Cp(CO)_3Mo\}_4Sn_4Te_6]$/New Organometallic Tin-Tellurium Compounds. Syntheses and Crystal Structures of $[\{Cp(CO)_2Fe\}_4Sn_2Te_2]$, $[\{Cp(CO)_3Mo\}_4Sn_2Te_2]$ and $[\{Cp(CO)_3Mo\}_4Sn_4Te_6]$. *Z. Naturforsch. B* **1994**, *49* (5), 621−626.
(38) Zingaro, R. A. Tributylphosphine Telluride. *J. Organomet. Chem.* **1963**, *1* (2), 200.
(39) So, J.-H.; Boudjouk, P. Convenient Syntheses of Hexamethyldisilathiane and Tetramethyldisilathiane. *Synthesis* **1989**, *1989* (04), 306−307.
(40) DeGroot, M. W.; Taylor, N. J.; Corrigan, J. F. Molecular Nanocluster Analogues of CdSe/ZnSe and CdTe/ZnTe Core/Shell Nanoparticles. *J. Mater. Chem.* **2004**, *14* (4), 654.
(41) Spackman, M. A.; Jayatilaka, D. Hirshfeld Surface Analysis. *CrystEngComm* **2009**, *11* (1), 19−32.
(42) Spackman, P. R.; Turner, M. J.; McKinnon, J. J.; Wolff, S. K.; Grimwood, D. J.; Jayatilaka, D.; Spackman, M. A. CrystalExplorer: A Program for Hirshfeld Surface Analysis, Visualization and Quantitative Analysis of Molecular Crystals. *J. Appl. Crystallogr.* **2021**, *54* (3), 1006−1011.
(43) Sheldrick, G. M. Crystal Structure Refinement with SHELXL. *Acta Crystallographica Section C Structural Chemistry* **2015**, *71* (1), 3−8.
(44) Sheldrick, G. M. SHELXT − Integrated Space-Group and Crystal-Structure Determination. *Acta Crystallographica Section A Foundations and Advances* **2015**, *71* (1), 3−8.
(45) Dolomanov, O. V.; Bourhis, L. J.; Gildea, R. J.; Howard, J. A. K.; Puschmann, H. OLEX2: A Complete Structure Solution, Refinement and Analysis Program. *J. Appl. Crystallogr.* **2009**, *42* (2), 339−341.
(46) Peng, D.; Middendorf, N.; Weigend, F.; Reiher, M. An Efficient Implementation of Two-Component Relativistic Exact-Decoupling Methods for Large Molecules. *J. Chem. Phys.* **2013**, *138* (18), 184105.
(47) Franzke, Y. J.; Middendorf, N.; Weigend, F. Efficient Implementation of One- and Two-Component Analytical Energy Gradients in Exact Two-Component Theory. *J. Chem. Phys.* **2018**, *148* (10), 104110.
(48) Franzke, Y. J.; Weigend, F. NMR Shielding Tensors and Chemical Shifts in Scalar-Relativistic Local Exact Two-Component Theory. *J. Chem. Theory Comput.* **2019**, *15* (2), 1028−1043.
(49) Franzke, Y. J.; Holzer, C. Exact Two-Component Theory Becoming an Efficient Tool for NMR Shieldings and Shifts with Spin−Orbit Coupling. *J. Chem. Phys.* **2023**, *159* (18), 184102.
(50) Franzke, Y. J.; Treß, R.; Pazdera, T. M.; Weigend, F. Error-Consistent Segmented Contracted All-Electron Relativistic Basis Sets of Double- and Triple-Zeta Quality for NMR Shielding Constants. *Phys. Chem. Chem. Phys.* **2019**, *21* (30), 16658−16664.
(51) Visscher, L.; Dyall, K. G. Dirac-Fock Atomic Electronic Structure Calculations Using Different Nuclear Charge Distributions. *At. Data. Nucl. Data Tables* **1997**, *67* (2), 207−224.
(52) Filatov, M.; Zou, W.; Cremer, D. Spin-Orbit Coupling Calculations with the Two-Component Normalized Elimination of the Small Component Method. *J. Chem. Phys.* **2013**, *139* (1), No. 014106.
(53) Perdew, J. P.; Burke, K.; Ernzerhof, M. Generalized Gradient Approximation Made Simple. *Phys. Rev. Lett.* **1996**, *77* (18), 3865−3868.
(54) Adamo, C.; Barone, V. Toward Reliable Density Functional Methods without Adjustable Parameters: The PBE0 Model. *J. Chem. Phys.* **1999**, *110* (13), 6158−6170.
(55) Becke, A. D. A New Mixing of Hartree−Fock and Local Density-Functional Theories. *J. Chem. Phys.* **1993**, *98* (2), 1372−1377.
(56) Chai, J.-D.; Head-Gordon, M. Long-Range Corrected Hybrid Density Functionals with Damped Atom−Atom Dispersion Corrections. *Phys. Chem. Chem. Phys.* **2008**, *10* (44), 6615.
(57) Holzer, C. An Improved Seminumerical Coulomb and Exchange Algorithm for Properties and Excited States in Modern Density Functional Theory. *J. Chem. Phys.* **2020**, *153* (18), 184115.
(58) Holzer, C.; Franzke, Y. J.; Kehry, M. Assessing the Accuracy of Local Hybrid Density Functional Approximations for Molecular Response Properties. *J. Chem. Theory Comput.* **2021**, *17* (5), 2928−2947.
(59) Armbruster, M. K.; Weigend, F.; van Wüllen, C.; Klopper, W. Self-Consistent Treatment of Spin−Orbit Interactions with Efficient Hartree−Fock and Density Functional Methods. *Phys. Chem. Chem. Phys.* **2008**, *10* (13), 1748.
(60) Reiter, K.; Mack, F.; Weigend, F. Calculation of Magnetic Shielding Constants with Meta-GGA Functionals Employing the Multipole-Accelerated Resolution of the Identity: Implementation and Assessment of Accuracy and Efficiency. *J. Chem. Theory Comput.* **2018**, *14* (1), 191−197.
(61) Pollak, P.; Weigend, F. Segmented Contracted Error-Consistent Basis Sets of Double- and Triple-ζ Valence Quality for One- and Two-Component Relativistic All-Electron Calculations. *J. Chem. Theory Comput.* **2017**, *13* (8), 3696−3705.
(62) Pausch, A. Consistent Analytical Second Derivatives of the Kohn−Sham DFT Energy in the Framework of the Conductor-Like Screening Model through Gaussian Charge Distributions. *J. Chem. Theory Comput.* **2024**, *20* (8), 3169−3183.
(63) Kehry, M.; Franzke, Y. J.; Holzer, C.; Klopper, W. Quasirelativistic Two-Component Core Excitations and Polarisabilities from a Damped-Response Formulation of the Bethe−Salpeter Equation. *Mol. Phys.* **2020**, *118* (21−), No. e1755064.
(64) Caldeweyher, E.; Bannwarth, C.; Grimme, S. Extension of the D3 Dispersion Coefficient Model. *J. Chem. Phys.* **2017**, *147* (3), No. 034112.
(65) Developers' Version of TURBOMOLE V7.9 2024, a Development of University of Karlsruhe and Forschungszentrum Karlsruhe GmbH 1989−2007, TURBOMOLE GmbH, since 2007. Available from https://www.turbomole.org (retrieved December 5, 2026).
(66) Franzke, Y. J.; Holzer, C.; Andersen, J. H.; Begušić, T.; Bruder, F.; Coriani, S.; Della Sala, F.; Fabiano, E.; Fedotov, D. A.; Fürst, S.; Gillhuber, S.; Grotjahn, R.; Kaupp, M.; Kehry, M.; Krstić, M.; Mack, F.; Majumdar, S.; Nguyen, B. D.; Parker, S. M.; Pauly, F.; Pausch, A.; Perlt, E.; Phun, G. S.; Rajabi, A.; Rappoport, D.; Samal, B.; Schrader, T.; Sharma, M.; Tapavicza, E.; Treß, R. S.; Voora, V.; Wodyński, A.; Yu, J. M.; Zerulla, B.; Furche, F.; Hättig, C.; Sierka, M.; Tew, D. P.; Weigend, F. TURBOMOLE: Today and Tomorrow. *J. Chem. Theory Comput.* **2023**, *19* (20), 6859−6890.
(67) Berwe, H.; Haas, A. Thiastannacyclohexane $(R_2SnS)_3$ Und -adamantane $(RSn)_4S_6$ Synthesen, Eigenschaften Und Strukturen. *Chem. Ber.* **1987**, *120* (7), 1175−1182.
(68) Blecher, A.; Dräger, M.; Mathiasch, B. $MeSn_4Se_6$, Geometrie Und Schwingungsformen Eines Adamantan-Gerüstes Aus Zinn-Selen-Bindungen/$(MeSn)_4Se_6$, Geometry and Vibrational Modes of an Adamantane Framework Formed by Tin-Selenium Bonds. *Z. Naturforsch. B* **1981**, *36* (11), 1361−1367.
(69) Kobelt, D.; Paulus, E. F.; Scherer, H. Röntgenstrukturanalyse von Methylthiostannonsäure. *Acta Crystallogr., Sect. B: Struct. Sci.* **1972**, *28* (8), 2323−2326.
(70) Pirani, A. M.; Mercier, H. P. A.; Dixon, D. A.; Borrmann, H.; Schrobilgen, G. J. Syntheses, Vibrational Spectra, and Theoretical Studies of the Adamantanoid $Sn_4Ch_{10}^{4-}$ (Ch = Se, Te) Anions: X-Ray

https://doi.org/10.1021/acs.inorgchem.6c02451
Inorg. Chem. XXXX, XXX, XXX−XXX

Crystal Structures of $[18\text{-Crown-6-K}]_4[Sn_4Se_{10}]\cdot 5en$ and $[18\text{-Crown-6-K}]_4[Sn_4Te_{10}]\cdot 3en\cdot 2THF$. *Inorg. Chem.* **2001**, *40* (19), 4823−4829.
(71) Hauser, R.; Merzweiler, K. Synthese und Kristallstruktur von $[Na_3(H_2O)_{6,5}(EtOH)][PhSnS_3]\cdot 3$ EtOH. *Z. anorg. allg. Chem.* **1998**, *624* (1), 10−12.
(72) Rinn, N.; Guggolz, L.; Hou, H. Y.; Dehnen, S. Systematic Access of Ternary Organotetrel-Copper Chalcogenide Clusters by $[PhTE_3]^{3-}$ Anions (T = Si, Sn; E = S, Se). *Chem.—Eur. J.* **2021**, *27* (43), 11167−11174.

https://doi.org/10.1021/acs.inorgchem.6c02451
Inorg. Chem. XXXX, XXX, XXX−XXX